GDCh Research Article Angewandte International Edition Chemie www.angewandte.org

How to cite: *Angew. Chem. Int. Ed.* **2025**, *64*, e202421259
doi.org/10.1002/anie.202421259

Metal Sulfide Clusters

Sequential Infiltration Synthesis of Cadmium Sulfide Discrete Atom Clusters

*Nuwanthaka P. Jayaweera, Shana Havenridge, Ashley R. Bielinski, Kihoon Kim, Niklas B. Thompson, Justin M. Hoffman, Amelia M. Wheaton, Prasenjit Sarkar, Rajesh Pathak, Jeffrey W. Elam, Cong Liu, Karen L. Mulfort, and Alex B. F. Martinson**

Abstract: Exposure of soft material templates to alternating volatile chemical precursors can produce inorganic deposition *within* the permeable template (e.g. a polymer thin film) in a process akin to atomic layer deposition (ALD). While such sequential infiltration synthesis (SIS) processes have now been demonstrated for many metal oxides, we report an SIS process for a transition metal sulfide – CdS. Gas phase dimethyl cadmium and hydrogen sulfide precursors infiltrated into poly(4-vinylpyridine) thin films result in the 3D-nucleation of clusters consistent with a cubane-type Cd_4S_4 core that are variably terminated with methyl, thiol and hydroxy capping ligands. First principles models and simulation of few-atom Cd-based clusters are consistent with electronic and vibrational spectroscopy and grazing-incidence total X-ray scattering measurements of 3D-cluster-arrays synthesized at 80 °C. The direct synthesis of few-atom transition metal sulfide clusters within polymer thin films will provide a versatile new route to precision architectures for light-absorbing materials including solar energy harvesting and conversion applications.

Introduction

Discrete nanoclusters (NCs) exhibit opto-electronic properties that are distinct from their corresponding bulk materials. As with small molecules, NC properties are a function of atom count, connectivity, and the resulting electronic structure. In contrast to larger nanoparticles (>2 nm), NCs may present surface atom configurations that are otherwise inaccessible and/or unstable in bulk material and surfaces. The unique properties of NCs and the potential for NC arrays with narrow size distributions to advance the field of (photo)(electro)catalysis are well documented.[1–11] For example, their homogeneous compositions and surfaces may allow for novel absorption transitions and afford new opportunities for efficient charge transfer in solar energy harvesting applications.[12–15]

However, the established routes for solution phase synthesis of clusters produce clusters with a broad size distribution and poor surface homogeneity which may involve additional purification steps to isolate homogeneous NC populations.[16–22] Furthermore, the present methods for the deposition of uniform NC arrays are largely restricted to quadrupole mass-selected soft landing[23–25] and the concentration of solution-synthesized NCs into thin films, both of which have incomplete control and issues with scalability.

Over the past decade, Sequential Infiltration Synthesis (SIS) has been developed as a route to incorporate metal oxide materials into soft material templates including a wide range of polymers.[26–31] SIS is an adaptation of Atomic Layer Deposition (ALD), a surface synthesis technique that is now used prolifically to realize thin film growth with precise control over the resulting material phase, thickness, and conformality.[26] In SIS, gas-phase metal organic precursor molecules permeate a soft material to reversibly adduct (or slowly and irreversibly react) with a polymer matrix. Specific functional groups present in the polymer matrix can act as initial adduction sites until introduction of a complementary precursor that may react to nucleate a small inorganic cluster with reduced volatility. Additional alternating exposure cycles may result in the nucleation of new clusters and/or in the growth of existing clusters. The spatial distribution and concentration of clusters in the polymer

[*] N. P. Jayaweera, A. R. Bielinski, K. Kim, A. B. F. Martinson
Material Science Division
Argonne National Laboratory
9700 South Cass Avenue, Lemont, Illinois, 60439, United States
E-mail: martinson@anl.gov

S. Havenridge, N. B. Thompson, A. M. Wheaton, P. Sarkar, C. Liu, K. L. Mulfort
Chemical Science and Engineering Division
Argonne National Laboratory
9700 South Cass Avenue, Lemont, Illinois, 60439, United States

J. M. Hoffman
X-ray Science Division
Argonne National Laboratory
9700 South Cass Avenue, Lemont, Illinois, 60439, United States

R. Pathak, J. W. Elam
Applied Materials Division
Argonne National Laboratory
9700 South Cass Avenue, Lemont, Illinois, 60439, United States

matrix may be controlled by adjusting nucleation and growth parameters during the SIS procedure. Further increasing the materials palette for, and our understanding of, SIS processes will enhance our ability to create functional materials with tailored properties.

Numerous groups have investigated cadmium chalcogenide (CdE) clusters using solution phase synthesis methods and theory calculations.[32–55] Solution phase synthesis methods often lead to broad size distributions, are challenging to isolate, and suffer from limited stability. Moreover, small CdE clusters with less than 10 cadmium atoms have been found to be especially challenging to synthesize and require air-free reaction conditions.[56]

In this study, we demonstrate the rapid synthesis of 3D-arrays of discrete Cd_xS_y clusters in poly(4-vinylpyridine) (P4VP) thin films using highly volatile dimethyl cadmium and hydrogen sulfide precursors. SIS parameters including precursor exposure, temperature, and the purge time between exposures are varied to investigate the range of accessible NC size, surface termination, uniformity, and the spatial distribution of deposition. Combining experimental and theoretical techniques, we describe the synthesis of molecular Cd_4S_4 core cubane type clusters with heterogeneous anionic capping ligands that include methyl, thiol and hydroxyl groups. The clusters are further stabilized by the presence of neutral capping ligands including pyridine as provided by the surrounding P4VP polymer matrix. The new SIS process considerably expands the number of metal sulfide SIS processes[57] and vapor phase synthesis routes to molecular inorganic clusters.[57–59]

Results and Discussion

Analysis of Cluster Synthesis Pathways by UV/Vis and PL Spectroscopies

A simple reaction scheme, shown in Scheme 1, is hypothesized to be the first in a sequence of reactions to form Cd_xS_y NCs. DFT calculations (see below) suggest that DMCd first favorably adducts to pyridine on the P4VP backbone before reacting with H_2S in the subsequent exposure to produce a methylcadmium thiol and release methane.

Multiple exposures of either DMCd or H_2S alone were not sufficient to produce NC absorbance, while nine complete SIS cycles at 80°C produced intense absorbance and PL (see Figure S1). Reflection-corrected absorbance measurements collected with a diffuse reflectance accessory (DRA) reveal that the resulting deposition has strong absorbance at 274 nm that steadily increases with the number of SIS cycles, Figure 1. A normalized overlay of the absorbance at variable SIS cycle numbers reveals similar spectral shapes including the 274 nm peak, a shoulder near 350 nm, and a sharp deep-UV peak that steadily decreases in relatively intensity with greater cycle number. In contrast, in the absence of a polymer template, alternating exposure of a solid substrate to the same precursors has been shown to produce polycrystalline zincblende and wurtzite CdS thin films from 100 to 300 °C.[60,61] Absorbance measurements readily distinguish the cluster deposition from thin films of CdS that exhibit band gap absorption from 2.3–2.4 eV (517–540 nm).

The PL emission of the clusters is centered at 520 nm, Figure 1c, and is relatively unchanging with increasing SIS cycle numbers observed in the normalized PL lineshape, Figure 1d. The consistent PL energy and linewidth further indicate an increasing density of Cd-based clusters without significant change in cluster size or structure. Together, the optical properties suggest that additional SIS cycles increase the cluster array density without significantly changing the character of the clusters. Increasing the growth temperature consistently reduces the absorbance and PL intensity of the resulting cluster array (Figure S2). The decreased absorbance and PL with higher growth temperature is consistent with a lower density of clusters that may result from faster desorption and diffusion of DMCd adducted within the P4VP polymer film during the DMCd purge step, prior to

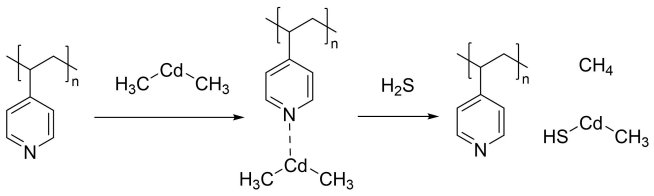

Scheme 1. P4VP-based cluster nucleation via adduct formation and subsequent reaction with H_2S.

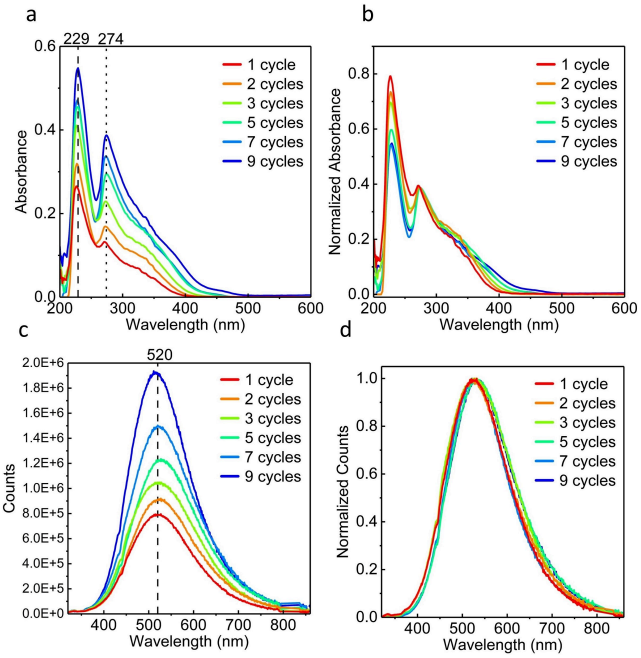

Figure 1. UV/Visible absorbance and photoluminescence (PL) spectra collected after complete SIS processing (1 to 9 cycles) at 80 °C. **a)** Reflection-corrected absorbance further corrected for small differences in the original polymer thickness **b)** absorbance normalized at 274 nm **c)** PL spectra corrected for small differences in the original polymer thickness **d)** PL spectra normalized at 520 nm

H_2S exposure. The spectral line shapes of both absorbance and PL slowly evolve with increasing temperature, suggesting that the SIS reaction mechanism may also be moderately sensitive to growth temperature.

Grazing Incidence Total X-ray Scattering (GITXS) Pair Distribution Function (PDF) Analysis.

The relative size of the Cd-based cluster was obtained through synchrotron-based total X-ray scattering measurements. In total X-ray scattering, both long-range and short-range atomic ordering are observed as Bragg diffraction and diffuse scattering, respectively, which together comprise the structure function of the measured material. Fourier transformation of the structure function produces the atomic PDF that describes the probability of finding two atoms separated by a given distance in real space. These films have low Cd-based cluster volume percentage (less than 6 atomic % of Cd according to XPS) relative to the organic polymer film matrix. This, combined with the low total volume of the 180-nm-thick film, presents a challenge to acquiring transmission scattering data with a sufficient signal-to-noise ratio for PDF analysis. Performing the data acquisition in grazing-incidence geometry allows for surface-sensitive data acquisition and significant signal enhancement, allowing for PDF analysis of the Cd_xS_y cluster.[6259]

The scattering from the glass substrate and pristine polymer film were subtracted from the total signal, leaving only the signal from the Cd_xS_y cluster data. After Fourier transformation, the PDF patterns of Cd_xS_y cluster samples reveal several consistent real space distances with high probability, Figure 2 (see Figure S3 for more information). The most common pairwise interaction observed in all samples occurs at ~2.5 Å, a spacing similar to known Cd–S bond lengths.[51,63,64] Even after a single SIS cycle, the 2.5 Å pair correlation distance is observed, despite moderate signal-to-noise due to low cluster density. Typical Cd–Cd distances for bulk CdS, quantum dots, and ultra small nanoparticles are ~4.1 Å.[51,63–66] The Cd_xS_y clusters in this study also show a feature close to 4.1 Å. A lack of prominent pairwise interactions at correlation distances greater than 7 Å suggests the absence of larger clusters or bulk-like CdS. The experimental radial PDF response may be further compared to the atom distances observed in simulated cluster structures optimized by DFT. Through this analysis, clusters containing more than five Cd atoms can be excluded from further consideration since pair correlations longer than ~7 Å are not observed experimentally. Experimental pair correlations less than ~7 Å also exclude the possibility of significant volume of bulk CdS, quantum dots, and ultra small nanoparticles that are expected to show Bragg diffraction and/or pair correlations >15 Å. Simulations of thiol-capped Cd-based clusters with two to five Cd atoms show the closest agreement to experimental Cd–Cd pair distances (Figure S4). The average Cd–Cd distance computed by DFT is approximately 4.1 Å for a four-atom Cd_xS_y cluster, most closely matching the experiment measurements. It should be noted that the peak around 4.1 Å is broader in the experimental data relative to the simulated data, implying a distribution of phases instead of a single precise structure. As a result, it appears that the NC population has structures of ~4 Cd atoms and may exhibit some distribution of phases, though this remains consistent across different SIS cycles and samples.

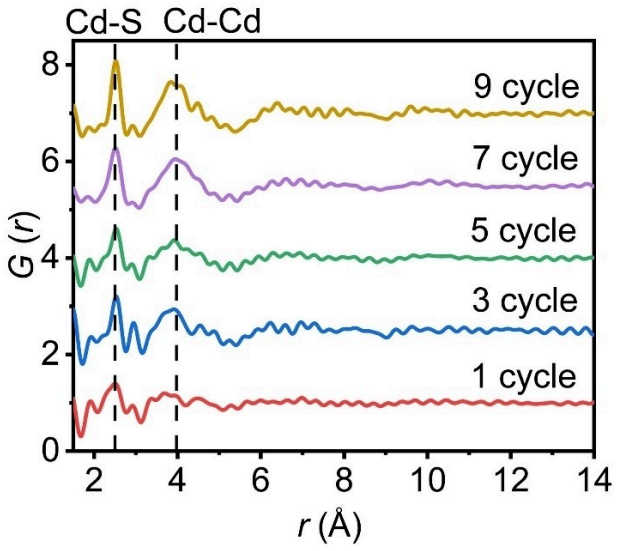

Figure 2. X-ray Total Scattering PDF Analysis Pair distribution functions (PDFs) from grazing-incidence total x-ray scattering for samples with different numbers of SIS cycles.

Three simulated Cd_4S_4 core clusters with diverse capping ligands (Figure 3) were examined in additional detail. The feasibility of these potential ligand environments will be further explored in the XPS and theoretical sections; however, DFT optimization is used to investigate how NCs′ ligand environment may affect core-atom distances. The simulated PDF patterns are similar; however, the core of the four-atom NCs is predicted to slightly decrease as the ligand is changed from methyl capped to thiol capped to hydroxyl capped based on DFT calculations.

XPS Depth Analysis

Compositional and chemical information of the P4VP-embedded Cd_xS_y clusters was deduced from XPS measurements of samples prepared in an ALD tool that is coupled to an inert gas glovebox. From the glovebox, the SIS cluster samples were transported to the XPS load-lock using an air-free transfer stage. Elemental analysis performed as a function of Ar-sputtering depth reveals that the average S/Cd ratio for all SIS cycle number samples is close to 1.5, Figure 4. A S/Cd ratio of ~1.5 is consistent with a Cd_4S_4 core with, on average, a 50:50 mixture of thiol and methyl or hydroxyl termination. (See Figure S5 for more information on XPS analysis) The distribution of Cd_xS_y clusters is hypothesized to be controlled by a complex interplay of vapor diffusion, precursor-polymer adduction, dissociation,

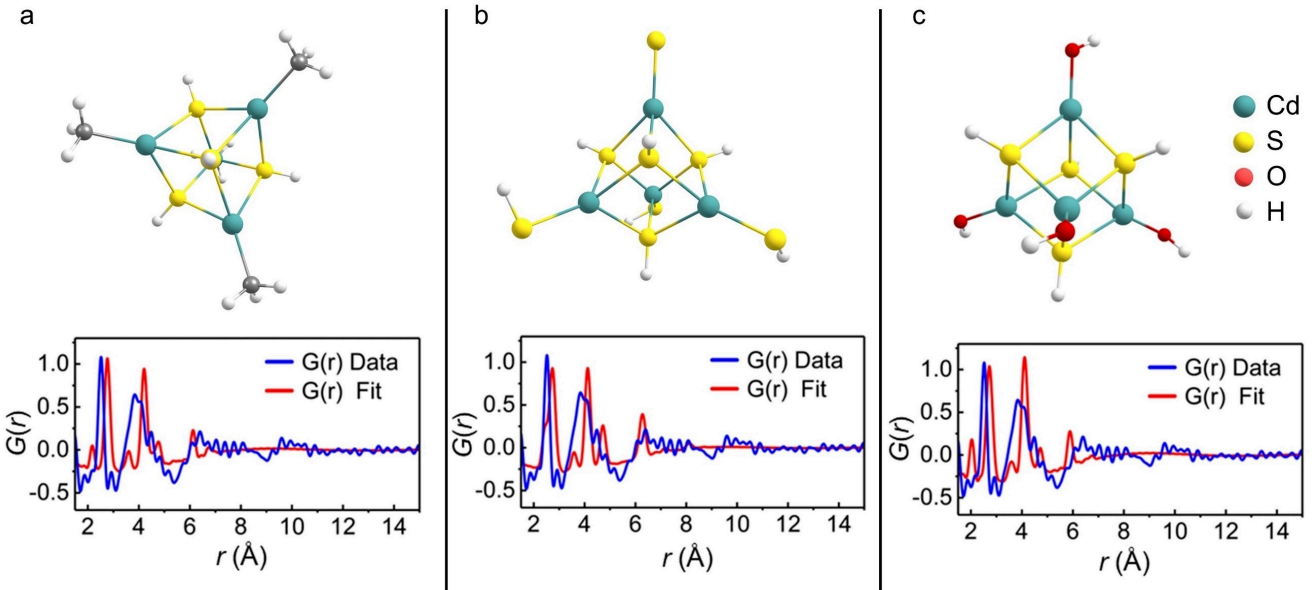

Average Cd-Cd distance Å	Average Cd-S distance Å	Average Cd-Cd distance Å	Average Cd-S distance Å	Average Cd-Cd distance Å	Average Cd-S distance Å
4.20 ± 0.00	2.76 ± 0.00	4.12 ± 0.01	2.66 ± 0.13	4.10 ± 0.03	2.73 ± 0.06

Figure 3. DFT optimized structure, PDF simulated patterns and average bond lengths from calculations at the B3LYP-D3/CEP-121G level of theory for **a**) methyl capped **b**) thiol capped **c)** hydroxyl capped Cd_4S_4 core NCs.

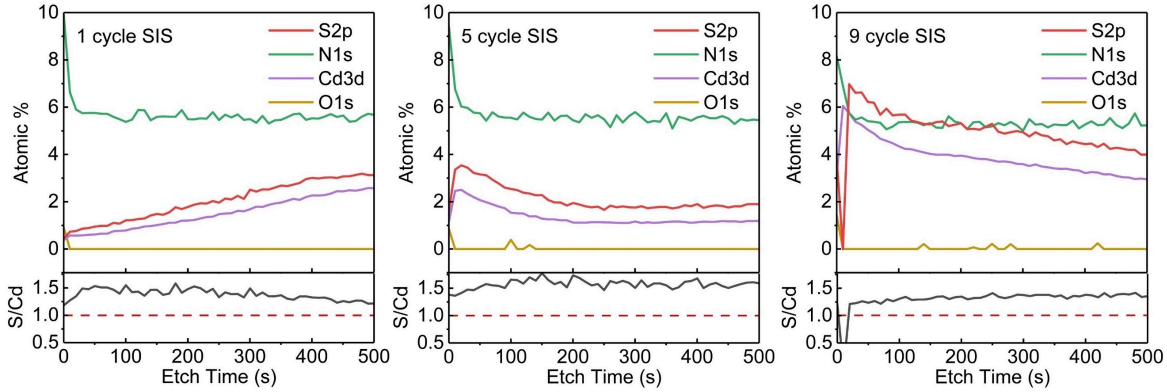

Figure 4. XPS depth analysis of elemental composition. (**top**) Atomic percentages of Cadmium, Sulfur, Oxygen and Nitrogen in first 500 s etching of 1 cycle, 5 cycle and 9 cycle SIS processed samples (**bottom**) Sulfur to Cadmium atomic ratio of 1 cycle, 5 cycle and 9 cycle SIS processed samples.

and diffusion out of the polymer prior to reaction with H_2S that, together, control cluster nucleation.

Computationally Informed Growth Mechanism

To aid the identification and characterization of experimental Cd_xS_y nanoclusters, DFT was used to optimize nanocluster models and analyze the possible growth mechanisms with and without the polymer. To reduce the number of possible conformations and sizes, as well as to improve mechanistic relevance, the reaction pathway is assumed to proceed through addition of single $Cd(SH)(CH_3)$ or $Cd(SH)_2$ species, Figure 5 and Figure S6, respectively. Computational studies on the geometry of CdSe NCs, specifically Cui, et. al's work that describes the stable high symmetry conformations of CdSe nanoclusters, also served to narrow the list of plausible conformations.[56] NCs were additionally optimized with different ratios of H_2S release (see Figure S6).

A potential mechanism may also be considered by evaluation of DFT thermodynamics. For example, it is

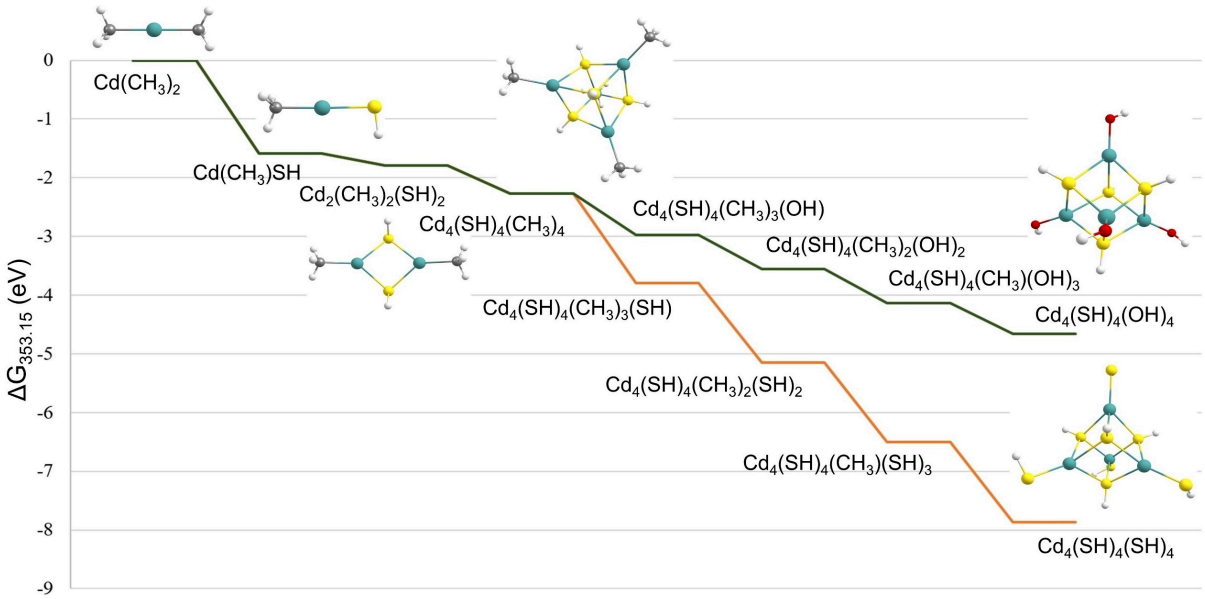

Figure 5. Calculated reaction free energy diagram for formation of possible Cd_4S_4 core clusters. NCs at the B3LYP-D3/CEP-121G level of theory at 80 °C.

favorable to produce all three terminations of the Cd_4S_4 core NC at 80 °C (e.g. CH_3, OH, and SH terminations) from the $Cd(CH_3)_2$ precursor. However, it is not favorable to produce OH terminated NC from SH terminated NC. In other words, the methyl terminated NC is a vital intermediate in the mechanism. This may lead to heterogeneity, including a mixture of SH and CH_3 terminated Cd_4S_4 core NCs in the polymer matrix. We hypothesize that methyl capped clusters could further oxidize in the presence of atmospheric water to form hydroxyl capped cluster forms as illustrated in Figure 5.

TDDFT calculations also allow calculation of theoretical absorption spectra for comparison to the experimental absorption spectra described above, see Figure 2. The simulated absorption spectra for cubic cadmium clusters with variable ligand termination each exhibit a characteristic absorption peak near 300 nm, Figure S7. The characteristic peak is at 286 nm in the methyl terminated NC, but slightly red shifted (lower energy) in the –SH and –OH terminated species, to 290 nm and 302 nm, respectively. The computations provide a reasonable match to the primary experimental absorption peak at 274 nm, see Figure S7, suggesting only a slight underestimation of the energy of this transition. However, the absorption peak in the experimental spectra is significantly broader than in the simulated spectra, especially at lower energy. As such, we hypothesize that a mixture of NCs with different ligand terminations may be present, with a majority terminated by CH_3 and SH. The methyl terminated cluster has the largest HOMO–LUMO (HL) gap of the three with a value of 4.85 eV, while the thiol terminated has the smallest HL gap of 3.67 eV. While no dynamics are modelled explicitly in our calculations, a smaller HL gap suggests that the electrons could be more susceptible to reactions. Therefore, even though the SH NC has a large formation energy from the CH_3 NC (Figure 5), we hypothesize that the CH_3 terminated clusters may be less susceptible to reactions, effectively reducing the concentration of SH capped NCs.

The primary absorption peak of all simulated cubic clusters has mixed ligand to metal charge transfer (LMCT) character. Each has an occupied molecular orbital that has large p atomic orbital contribution on the sulfurs inside the cube, as well as a small amount of extra-cluster ligand character. This transitions into a molecular orbital that is mostly from d orbitals on the Cd atoms (see Figure S8–S10). All three NCs are also predicted to exhibit a higher energy absorption feature where the excitations that produce large oscillator strengths are close to the experimental peak of 229 nm, the closest being those with SH and OH termination. The methyl terminated NC has similar transitions in the high energy range, but they are blue shifted compared to that of the SH and OH NCs, with the strongest excitation at a value of 205 nm.

FTIR Characterization of the Clusters

Comparison of the infrared spectrum for a 100 cycle Cd_xS_y SIS sample to a P4VP (no SIS) control reveals a new interaction between the polymer and Cd_xS_y cluster, Figure 6. Simulation of the vibrational spectra suggests that the new peak at 1017 cm^{-1} corresponds to expanding and contracting in the pyridine ring and Cd–N stretching. The shoulder peak next to 1615 cm^{-1} is related to a symmetric stretch between opposite carbon bonds in the pyridine ring ligand which is disturbed by the new Cd–N interaction. For simplicity, the simulation assumes that 100 % of pyridine-sites on the polymer are bound to a Cd_4S_4-core cluster. However, a much lower pyridine site occupancy is expected, even after 100 SIS cycles. Therefore, a much smaller perturbation in

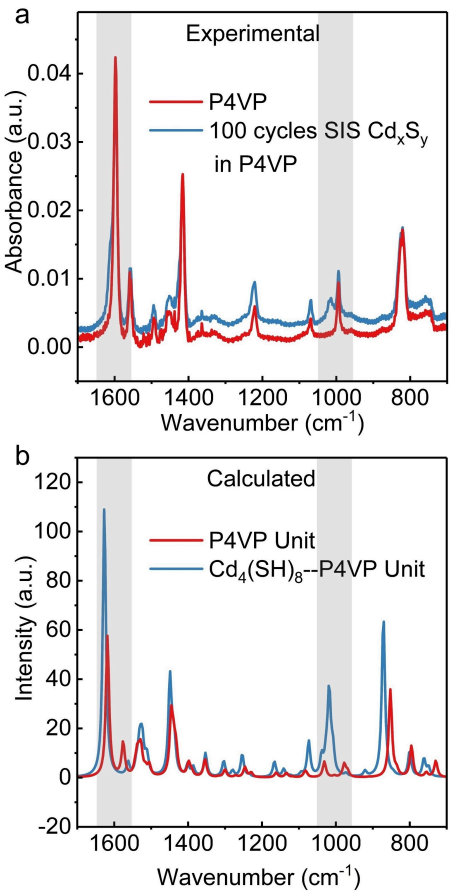

Figure 6. Experimental vs calculated FTIR spectra comparison before and after SIS processing at 80 °C in P4VP matrix. **a)** Experimental P4VP and 100 cycle SIS spectra **b)** DFT calculated P4VP unit and $Cd_4(SH)_8$ P4VP one unit adduct at the B3LYP-D3/CEP-121G level of theory. The grey areas highlight infrared energies where significant intensity changes are simulated and observed.

the experimental spectra after SIS treatment is expected, as full coordination of all pyridines is unlikely in the dilute conditions used for cluster synthesis.

Conclusion

Alternating exposure of a poly(4-vinylpyridine) polymer thin film to dimethyl cadmium and hydrogen sulfide precursors incorporates inorganic CdS within the polymer via a low temperature SIS process. Evidence for few-atom cadmium sulfide clusters within the polymer thin film include dramatically blue-shifted optical absorption and a lack of pair correlations beyond 7 Å. Simulated Cd_4S_4 core cubane type clusters with heterogeneous capping ligands are most consistent with combined experimental and computational structure studies. Thermodynamic consideration of DFT calculations reveal that the formation of methyl-capped and thiol-capped clusters is possible under inert atmosphere synthesis conditions. Pyridine functions as a neutral ligand in the polymer backbone and is hypothesized to passivate the cluster cores. The facile SIS of transition metal sulfide clusters allows excess precursors and by-products to be quickly eliminated through purging under low vacuum and avoids the difficult and lengthy purification procedures needed for the solution phase syntheses of discrete atom clusters. This route to discrete atom clusters may enable the synthesis of novel solar energy-absorbing materials with well-defined structures and unique properties.

Acknowledgements

This work was supported by the U.S. Department of Energy, Office of Science, Office of Basic Energy Sciences, Division of Chemical Sciences, Geosciences, and Biosciences at Argonne National Laboratory under Contract No. DE-AC02-06CH11357. The authors gratefully acknowledge the computing resources provided on Bebop; a high-performance computing cluster operated by the Laboratory Computing Resource Center at Argonne National Laboratory. We acknowledge DESY (Hamburg, Germany), a member of the Helmholtz Association HGF, for the provision of experimental facilities for total scattering. Parts of this research were carried out at PETRA III and we would like to thank Ann-Christin Dippel and Fernando I. Saldana for assistance in using the grazing-incidence setup at beamline P21.1. Beamtime was allocated for proposal I-20231362.

Conflict of Interest

The authors declare no conflict of interest.

Data Availability Statement

The data that support the findings of this study are available from the corresponding author upon reasonable request.

Keywords: atomic layer deposition · metal chalcogen · sequential infiltration synthesis · semiconductors · thin films

[1] A. T. Bell, *Science* **2003**, *299*, 1688–1691.
[2] S. Vajda, M. G. White, *ACS Catal.* **2015**, *5*, 7152–7176.
[3] G. A. Somorjai, J. Y. Park, *Top. Catal.* **2008**, *49*, 126–135.
[4] X. Lai, T. P. St. Clair, M. Valden, D. W. Goodman, *Prog. Surf. Sci.* **1998**, *59*, 25–52.
[5] M. Haruta, M. Daté, *Appl. Catal. Gen.* **2001**, *222*, 427–437.
[6] Q. Fu, H. Saltsburg, M. Flytzani-Stephanopoulos, *Science* **2003**, *301*, 935–938.
[7] A. Corma, H. Garcia, *Chem. Soc. Rev.* **2008**, *37*, 2096–2126.
[8] M. O. J. Jäger, E. V. Morooka, F. Federici Canova, L. Himanen, A. S. Foster, *Npj Comput. Mater.* **2018**, *4*, 1–8.
[9] G. Prieto, H. Tüysüz, N. Duyckaerts, J. Knossalla, G.-H. Wang, F. Schüth, *Chem. Rev.* **2016**, *116*, 14056–14119.
[10] Y. Wang, X. Xu, W. Lu, Y. Huo, L. Bian, *Dalton Trans.* **2018**, *47*, 4219–4227.
[11] W. Baek, M. S. Bootharaju, K. M. Walsh, S. Lee, D. R. Gamelin, T. Hyeon, *Nat. Mater.* **2021**, 1–8.
[12] H. Fang, P. Jena, *J. Phys. Chem. Lett.* **2016**, *7*, 1596–1603.

[13] P. Jena, Q. Sun, *Chem. Rev.* **2018**, *118*, 5755–5870.
[14] K. Xu, K. Chen, D. Xue, *Mater.* **2023**, *1*, 100030.
[15] Z. He, D. Wang, Q. Yu, M. Zhang, S. Wang, W. Huang, C. Luan, K. Yu, *ACS Omega* **2021**, *6*, 14458–14466.
[16] C.-A. J. Lin, T.-Y. Yang, C.-H. Lee, S. H. Huang, R. A. Sperling, M. Zanella, J. K. Li, J.-L. Shen, H.-H. Wang, H.-I. Yeh, W. J. Parak, W. H. Chang, *ACS Nano* **2009**, *3*, 395–401.
[17] Z. A. Peng, X. Peng, *J. Am. Chem. Soc.* **2002**, *124*, 3343–3353.
[18] Y. Shen, M. Y. Gee, R. Tan, P. J. Pellechia, A. B. Greytak, *Chem. Mater.* **2013**, *25*, 2838–2848.
[19] Y. Shen, A. Roberge, R. Tan, M. Y. Gee, D. C. Gary, Y. Huang, D. A. Blom, B. C. Benicewicz, B. M. Cossairt, A. B. Greytak, *Chem. Sci.* **2016**, *7*, 5671–5679.
[20] S. Singh, J. Leemans, F. Zaccaria, I. Infante, Z. Hens, *Chem. Mater.* **2021**, *33*, 2796–2803.
[21] L. Gou, C. J. Murphy, *Nano Lett.* **2003**, *3*, 231–234.
[22] N. P. Jayaweera, J. H. Dunlap, F. Ahmed, T. Larison, L. Buzoglu Kurnaz, M. Stefik, P. J. Pellechia, A. W. Fountain, A. B. Greytak, *Inorg. Chem.* **2022**, *61*, 10942–10949.
[23] W. Harbich, S. Fedrigo, F. Meyer, D. M. Lindsay, J. Lignieres, J. C. Rivoal, D. Kreisle, *J. Chem. Phys.* **1990**, *93*, 8535–8543.
[24] "Chiral enrichment of serine via formation, dissociation, and soft-landing of octameric cluster ions | Journal of the American Society for Mass Spectrometry," can be found under https://pubs.acs.org/doi/10.1016/j.jasms.2004.06.010, n/d.
[25] P. Fayet, F. Patthey, H.-V. Roy, Th. Detzel, W.-D. Schneider, *Surf. Sci.* **1992**, *269–270*, 1101–1108.
[26] R. Z. Waldman, N. Jeon, D. J. Mandia, O. Heinonen, S. B. Darling, A. B. F. Martinson, *Chem. Mater.* **2019**, *31*, 5274–5285.
[27] R. Z. Waldman, D. J. Mandia, A. Yanguas-Gil, A. B. F. Martinson, J. W. Elam, S. B. Darling, *J. Chem. Phys.* **2019**, *151*, 190901.
[28] A. Subramanian, N. Tiwale, C.-Y. Nam, *JOM* **2019**, *71*, 185–196.
[29] I. Weisbord, N. Shomrat, R. Azoulay, A. Kaushansky, T. Segal-Peretz, *Chem. Mater.* **2020**, *32*, 4499–4508.
[30] O. Yurkevich, E. Modin, I. Šarić Janković, R. Peter, M. Petravić, M. Knez, *Chem. Mater.* **2023**, *35*, 7529–7541.
[31] Y. Ren, E. K. McGuinness, C. Huang, V. R. Joseph, R. P. Lively, M. D. Losego, *Chem. Mater.* **2021**, *33*, 5210–5222.
[32] S. Kudera, M. Zanella, C. Giannini, A. Rizzo, Y. Li, G. Gigli, R. Cingolani, G. Ciccarella, W. Spahl, W. J. Parak, L. Manna, *Adv. Mater.* **2007**, *19*, 548–552.
[33] A. Kasuya, R. Sivamohan, Y. A. Barnakov, I. M. Dmitruk, T. Nirasawa, V. R. Romanyuk, V. Kumar, S. V. Mamykin, K. Tohji, B. Jeyadevan, K. Shinoda, T. Kudo, O. Terasaki, Z. Liu, R. V. Belosludov, V. Sundararajan, Y. Kawazoe, *Nat. Mater.* **2004**, *3*, 99–102.
[34] C. B. Murray, D. J. Norris, M. G. Bawendi, *J. Am. Chem. Soc.* **1993**, *115*, 8706–8715.
[35] T. Vossmeyer, L. Katsikas, M. Giersig, I. G. Popovic, K. Diesner, A. Chemseddine, A. Eychmueller, H. Weller, *J. Phys. Chem.* **1994**, *98*, 7665–7673.
[36] S. Behrens, M. Bettenhausen, A. Eichhöfer, D. Fenske, *Angew. Chem. Int. Ed. Engl.* **1997**, *36*, 2797–2799.
[37] K. Yu, M. Z. Hu, R. Wang, M. L. Piolet, M. Frotey, Md. B. Zaman, X. Wu, D. M. Leek, Y. Tao, D. Wilkinson, C. Li, *J. Phys. Chem. C* **2010**, *114*, 3329–3339.
[38] F. S. Riehle, R. Bienert, R. Thomann, G. A. Urban, M. Krüger, *Nano Lett.* **2009**, *9*, 514–518.
[39] J. Ouyang, Md. B. Zaman, F. J. Yan, D. Johnston, G. Li, X. Wu, D. Leek, C. I. Ratcliffe, J. A. Ripmeester, K. Yu, *J. Phys. Chem. C* **2008**, *112*, 13805–13811.
[40] Z.-J. Jiang, D. F. Kelley, *ACS Nano* **2010**, *4*, 1561–1572.
[41] Q. Dai, D. Li, J. Chang, Y. Song, S. Kan, H. Chen, B. Zou, W. Xu, S. Xu, B. Liu, G. Zou, *Nanotechnology* **2007**, *18*, 405603.
[42] N. Herron, J. C. Calabrese, W. E. Farneth, Y. Wang, *Science* **1993**, *259*, 1426–1428.
[43] J. F. Corrigan, O. Fuhr, D. Fenske, *Adv. Mater.* **2009**, *21*, 1867–1871.
[44] A. Eichhöfer, O. Hampe, M. Blom, *Eur. J. Inorg. Chem.* **2003**, *2003*, 1307–1314.
[45] "A 'Double-Diamond Superlattice' Built Up of Cd17S4(SCH2CH2OH)26 Clusters | Science," can be found under https://www.science.org/doi/10.1126/science.267.5203.1476, **n.d**.
[46] B. M. Cossairt, P. Juhas, S. J. L. Billinge, J. S. Owen, *J. Phys. Chem. Lett.* **2011**, *2*, 3075–3080.
[47] B. M. Cossairt, J. S. Owen, *Chem. Mater.* **2011**, *23*, 3114–3119.
[48] C. Xu, Z. Zhou, H. Han, *Crystals* **2022**, *12*, 1236.
[49] N. Kumar, F. Alam, V. Dutta, *RSC Adv.* **2016**, *6*, 28316–28321.
[50] D. R. Nevers, C. B. Williamson, T. Hanrath, R. D. Robinson, *Chem. Commun.* **2017**, *53*, 2866–2869.
[51] C. B. Williamson, D. R. Nevers, A. Nelson, I. Hadar, U. Banin, T. Hanrath, R. D. Robinson, *Science* **2019**, *363*, 731–735.
[52] L. Li, J. Zhang, M. Zhang, N. Rowell, C. Zhang, S. Wang, J. Lu, H. Fan, W. Huang, X. Chen, K. Yu, *Angew. Chem. Int. Ed.* **2020**, *59*, 12013–12021.
[53] H. Lei, L. Chen, L. Wang, *J. Phys. Chem. Lett.* **2023**, *14*, 5818–5826.
[54] S. Mazzotti, A. S. Mule, A. B. Pun, J. T. Held, D. J. Norris, *ACS Nano* **2023**, *17*, 13232–13240.
[55] H. H. Ripberger, K. J. Schnitzenbaumer, L. K. Nguyen, D. M. Ladd, K. R. Levine, D. G. Dayton, M. F. Toney, B. M. Cossairt, *J. Am. Chem. Soc.* **2023**, *145*, 27480–27492.
[56] Y. Cui, Z. Lou, X. Wang, S. Yu, M. Yang, *Phys. Chem. Chem. Phys.* **2015**, *17*, 9222–9230.
[57] K. Kim, S. Havenridge, N. J. Zaluzec, D. Kang, N. P. Jayaweera, J. W. Elam, K. L. Mulfort, C. Liu, A. B. F. Martinson, *ACS Nano* **2024**, *18*, 31372–31380.
[58] T. Kunene, A. B. F. Martinson, *J. Vac. Sci. Technol. A* **2023**, *41*, 042402.
[59] X. He, R. Z. Waldman, D. J. Mandia, N. Jeon, N. J. Zaluzec, O. J. Borkiewicz, U. Ruett, S. B. Darling, A. B. F. Martinson, D. M. Tiede, *ACS Nano* **2020**, *14*, 14846–14860.
[60] J. R. Bakke, H. J. Jung, J. T. Tanskanen, R. Sinclair, S. F. Bent, *Chem. Mater.* **2010**, *22*, 4669–4678.
[61] Y. Luo, D. Slater, M. Han, J. Moryl, R. M. Osgood, J. G. Chen, *Langmuir* **1998**, *14*, 1493–1499.
[62] A.-C. Dippel, M. Roelsgaard, U. Boettger, T. Schneller, O. Gutowski, U. Ruett, *IUCrJ* **2019**, *6*, 290–298.
[63] V. I. Korsounski, R. B. Neder, K. Hradil, C. Barglik-Chory, G. Müller, J. Neuefeind, *J. Appl. Crystallogr.* **2003**, *36*, 1389–1396.
[64] L. Tan, A. J. Misquitta, A. Sapelkin, L. Fang, R. M. Wilson, D. S. Keeble, B. Zhang, T. Zhu, F. S. Riehle, S. Han, K. Yu, M. T. Dove, *Nanoscale* **2019**, *11*, 21900–21908.
[65] X. Yang, A. S. Masadeh, J. R. McBride, E. S. Božin, S. J. Rosenthal, S. J. L. Billinge, *Phys. Chem. Chem. Phys.* **2013**, *15*, 8480–8486.
[66] R. B. Neder, V. I. Korsunskiy, *J. Phys. Condens. Matter* **2005**, *17*, S125.

Manuscript received: November 1, 2024
Version of record online: January 13, 2025